Fragmentation disrupts the seasonality of Amazonian evergreen forests

Matheus Nunes (matheus.nunes@helsinki.fi)
University of Helsinki

José Luís Camargo
Biological Dynamics of Forest Fragment Project (INPA & STRI) https://orcid.org/0000-0003-0370-9878

Grégoire Vincent
CIRAD

Kim Calders
Ghent University https://orcid.org/0000-0002-4562-2538

Rafael Oliveira
University of Campinas

Alfredo Huete
School of Life Sciences, University of Technology Sydney, NSW 2007

Yhasmin Moura
Karlsruhe Institute of Technology

Bruce Nelson
Brazil's National Institute for Amazon Research (INPA)

Marielle Smith
Michigan State University

Scott Stark
Michigan State University

Eduardo Maeda
University of Helsinki https://orcid.org/0000-0001-7932-1824

Biological Sciences - Article

Keywords: leaf phenology, forests, Amazonian forests, forest fragmentation and loss

Posted Date: July 29th, 2021

DOI: https://doi.org/10.21203/rs.3.rs-722038/v1

Version of Record: A version of this preprint was published at Nature Communications on February 17th, 2022. See the published version at https://doi.org/10.1038/s41467-022-28490-7.

Fragmentation disrupts the seasonality of Amazonian evergreen forests

Authors

Matheus H. Nunes [1, 11], José Luis C. Camargo [2], Grégoire Vincent [3], Kim Calders [4], Rafael S. Oliveira [5], Alfredo Huete [6], Yhasmin Mendes de Moura [7, 8], Bruce Nelson [9], Marielle N. Smith [10], Scott C. Stark [10], Eduardo E. Maeda [1]

[1] Department of Geosciences and Geography, University of Helsinki, Helsinki, 00014, Finland

[2] Biological Dynamics of Forest Fragment Project, National Institute for Amazonian Research, Manaus, AM, 69067-375 Brazil

[3] AMAP, Univ Montpellier, IRD, CIRAD, CNRS, INRAE, Montpellier, France

[4] CAVElab – Computational and Applied Vegetation Ecology, Department of Environment, Faculty of Bioscience Engineering, Ghent University, Ghent, Belgium

[5] Department of Plant Biology, Institute of Biology, University of Campinas, Campinas, Brazil

[6] School of Life Sciences, Faculty of Science, University of Technology Sydney, Sydney, NSW 2007, Australia

[7] Institute of Geography and Geoecology, Karlsruhe Institute of Technology (KIT), Kaiserstr. 12, 76131, Karlsruhe, Germany

[8] Centre for Landscape and Climate Research, School of Geography, Geology and the Environment, University of Leicester, Leicester, LE17RH, United Kingdom

[9] National Institute of Amazonian Research, Manaus, Brazil

[10] Department of Forestry, Michigan State University, East Lansing, MI, USA

[11] Corresponding author (matheus.nunes@helsinki.fi)

ABSTRACT

Predictions of the magnitude and timing of leaf phenology in Amazonian forests remain highly controversial, which limits our understanding of future ecosystem function with a changing environment. Here, we use biweekly terrestrial LiDAR surveys spanning wet and dry seasons in Central Amazonia to show that plant phenology of old-growth forests varies strongly across strata but that this seasonality is sensitive to disturbances arising from forest fragmentation. In combination with continuous microclimate measurements, we found that when maximum daily temperatures reached 35 °C in the latter part of the dry season, the upper canopy of large trees in undisturbed forests shed their leaves and branches. By contrast, the understory greens-up with increased light availability driven by the upper canopy loss alongside more sunlight radiation, even during periods of drier soil and atmospheric conditions. However, persistently high temperatures on forest edges exacerbated the upper canopy losses of large trees throughout the dry season, and the understory seasonality in these light-rich environments was disrupted as a result of the altered canopy structure. These findings demonstrate the plant-climate interactions controlling the seasonality of wet Amazonian forests and show that forest fragmentation will aggravate forest loss under a hotter and drier future scenario.

INTRODUCTION

Leaf phenology of Amazonian forests is a key component controlling the exchange of energy and trace gases – water vapour, carbon dioxide and volatile organic compounds - with influences on vegetation feedbacks on the regional and global climates [1–5]. In the past decade, several studies have demonstrated from field data and remote sensing products that a majority of Amazonian forests respond to climatic variations [2,6]. There is also mounting evidence that evergreen canopies have a seasonal variation [7–11] with changes in leaf demography and canopy structure [12]. Long-term studies have shown that 60 - 70% of species of humid Amazonian forests flush new leaves in the dry months [12,13] linked to higher solar radiation [4,14], which leads to increases in gross primary productivity as a result of new young leaves with higher photosynthetic capacity and water-use efficiency [4,15,16]. However, when some Amazonian forests are impacted by water stress, leaf development is reduced [17], and trees shed their leaves, increasing litterfall [10,18], which interact to alter leaf area dynamics [19]. To complicate matters further, leaf phenology also responds to different gene expressions that have evolved to maximize photosynthetic and water use efficiency during the dry season, reduce plant competition for light and water, and minimise herbivore pressure [7,16,20–22].

The effects of climatic variations on leaf phenology can also be amplified by forest fragmentation [23]. Forest edges contain a large abundance of early successional species with rapid acquisition of resources that maximise new leaf production and growth [24,25], but may be more vulnerable to droughts [26]. Forest fragmentation can increase the evaporative demand due to higher temperatures and wind exposure, and soil moisture can be lower at fragment edges [27], which may cause leaves to drop and lead to higher branch turnover [12,23]. However, ground observations of litterfall in Amazonian forests have shown only a mild seasonality near edges [28]. Indeed, large uncertainty remains regarding the responses of fragmented forests to climatic seasonality, particularly because some species can benefit from higher solar radiation [29,30], drought resistance varies among species [31–33] and surviving trees may acclimate or be adapted to the drier, hotter conditions near edges [34]. As the number of contiguously forested areas are significantly decreasing in the Amazon [35], understanding the effects of forest fragmentation on phenology is vital for predicting the benefits of protecting non-fragmented Amazonian forest landscapes.

Seasonal variations in leaf quantity and leaf area across evergreen Amazonian forests have frequently been considered negligible or small [4,12,21,36]. However, spaceborne remote sensing approaches tend to detect only trees that dominate the upper canopy, thereby obtaining more information from those species that are adapted to more stressful conditions such as high solar radiation and temperatures and low air humidity [37]. LiDAR-based observations may provide fresh insights into the interacting factors controlling vegetation dynamics and have more recently shown that leaf phenology in Amazonian forests is stratified over canopy positions and conditions [19,38]. Here, we investigate the phenology of forests in Central Amazonia with terrestrial laser scanning (TLS, also terrestrial LiDAR) surveys collected every 15 days spanning the wet and dry seasons. We use TLS measurements to investigate how forest fragmentation and microclimatic seasonality interact to affect plant area of the understory and the upper canopy. Repeated TLS measurements can monitor subtle changes in forest structure in specific horizontal layers [42] (Figure 1). Furthermore, the detailed and precise structural measurements offered by this system can help answer fundamental questions about the three-dimensional (3D) ecology of trees [43] without suffering from potentially confounding artefacts present in passive optical satellite images [11,36]. Using a combination of 11 repeat TLS surveys, as well as continuous air temperature and soil moisture measurements in old-growth, undisturbed forests and fragmented forests under edge effects, we test: (1) whether vertically stratified plant phenology in undisturbed forests varies with microclimatic conditions, and (2) whether plant phenology is sensitive to disturbances arising from forest fragmentation. We predict that the hotter and drier conditions of edges exacerbate leaf loss during the dry season. To our knowledge, the work

presented in this paper is the first to analyse tropical forest phenology with high spatial- and temporal resolution 3D measurements and the first to experimentally demonstrate the effects of forest fragmentation on the seasonal variation of leaf area, and its vertical stratification, combined with microclimate measurements.

Figure 1. A view from the forest understory with colours depicting plants from distinct strata. The high speed terrestrial laser scanning (TLS) data acquisition of 500,000 measurements per second provides detailed measurements capable of detecting fine changes in the vegetation structure. We used a scan resolution of 40 mdeg in both azimuth and zenith directions, which results in a point spacing of 1.4 cm at 20 m distance from the scanner. The laser pulse repetition rate used was 600 kHz, allowing a measurement range of up to 350 m and up to eight returns per pulse.

RESULTS

Seasonal climatic trends in Central Amazonian forests

Daily precipitation estimates indicate the occurrence of a 4-month period of accumulated rainfall below 200 mm month^{-1}, and significant reductions in soil moisture between July and September in Central Amazonia (hereinafter referred to as “dry season”). This dry season was coincident with a period of high Photosynthetic Active Radiation (PAR, Figure 2a) and significant increases in temperature of the understory in the forest interior and fragment edges (Figures 2b and 2c). Forest

fragmentation led to higher temperatures in the edges, while water availability in the soil remained virtually unaffected by edge effects.

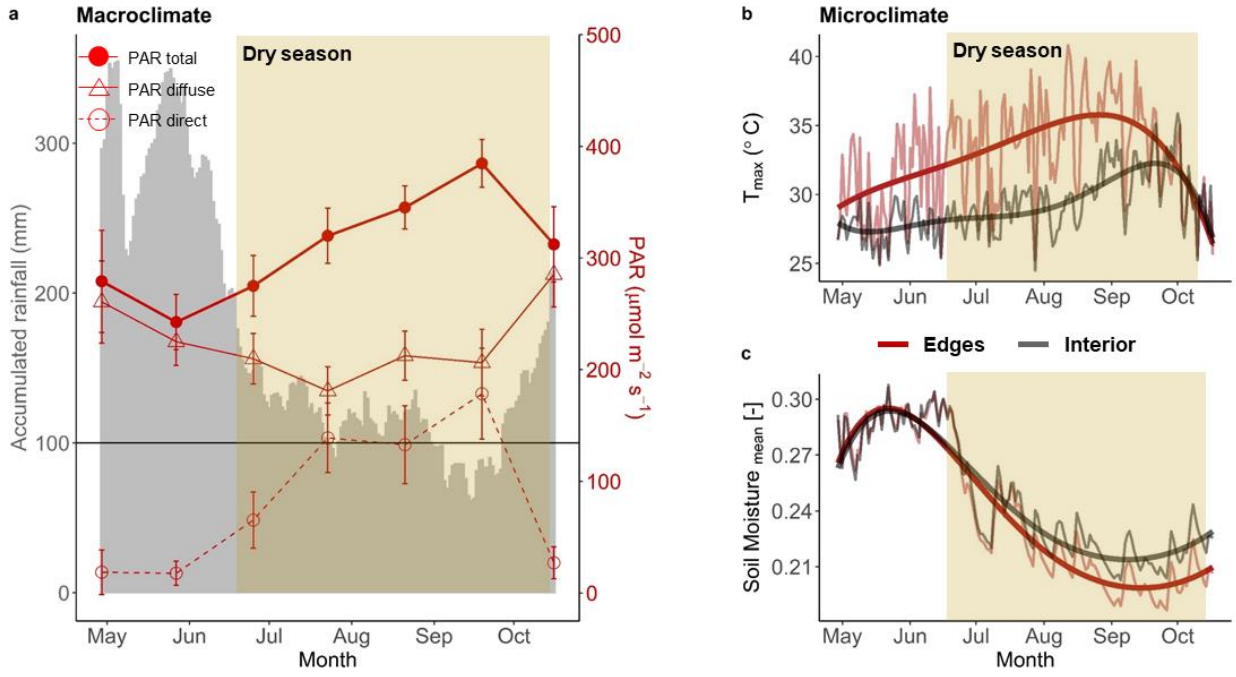

Figure 2. **Climatic seasonality in Central Amazonian forests**. a) Estimated diffuse, direct and total (diffuse + direct) Photosynthetic Active Radiation (PAR, in red) estimated from MODIS and accumulated 30-day (monthly) rainfall from NASA POWER (in grey area). Each red point represents the monthly average with error bars representing the 95% confidence intervals. Microclimate measurements in the understory of forest edges and interiors were continuously measured every 15 minutes. b) Maximum daily temperatures in the edge understory (red) and interior (dark grey) and c) mean daily soil moisture (as volumetric water soil content: cm^3 water/ cm^3 soil) measured in the edges (red) and in the interior of fragments (dark grey). Polynomial models of order 5 of the microclimate variables were generated as a smoothing line for visualization purposes. Dry season was defined as the period with accumulated monthly precipitation < 200 mm $month^{-1}$ when we observed the most pronounced reductions in soil moisture.

Seasonal PAI variation and fragmentation effects

The repeated high-resolution terrestrial LiDAR time-series revealed a strong vertical variability in the timing and magnitude of seasonal changes in the Plant Area Index (PAI) of old-growth forests

and forests under edge effects. The most parsimonious model to predict PAI for both the understory and upper canopy strata was the Eq. 3 model which includes the effects of season and edges on PAI, whereas the Eq. 4 model was selected for total PAI (without accounting for the vertical stratification). Note that the lack of time effect in Eq. 4 indicated that there is significant temporal variation in only the vertical distribution of PAI (Supplementary Table 1; Supplementary Figure 4).

$$PAI_{ij} = \beta_0 + \beta_1 time_{ij} \times edge\ effects_{ij} + u_i + e_{ij} \quad \text{(Eq. 3)}$$

$$PAI_{ij} = \beta_0 + \beta_1 edge\ effects_{ij} + u_i + e_{ij} \quad \text{(Eq. 4)},$$

where PAI_{ij} is the plant area index in transect i and time j, β_0 and β_1 is the fixed effect parameter, u_i is the random intercept for transect i, and e_{ij} is residual error.

In forest interiors, losses in the understory preceded the dry season, while significant losses in the upper canopy occurred at the end of the dry season (Figure 3, black). More specifically, the PAI of the understory declined rapidly between April and early June (t = -3.4; P value < 0.001) and reached a total 5.3% (-0.43 m^2 m^{-2}) decline by late July (t = -4.2; P value < 0.001) (Figure 3d). The PAI then increased to a full recovery (+ 0.43 m^2 m^{-2}) in September (t = -1.2; P value = 0.21). By contrast, the upper canopy layer showed an inverse seasonal pattern in comparison with the understory - the upper canopy PAI remained relatively stable from April to September, but experienced 7.6% (-0.25 m^2 m^{-2}) loss late September (t = -3.9; P value < 0.001) (Figure 3b).

The PAI time-series of forest edges (Figure 3, red) showed significantly distinct patterns in comparison with those observed in forests distant from edges (as the *time* x *edge* interaction term improved the model based on AIC; Supplementary Table 1). Despite a subtle decline in PAI between May and July of 2.6% (-0.08 m^2 m^{-2}) (Figure 3c), the PAI in the edge understory did not show significant seasonal changes (t = -1.7; P value = 0.07). However, the upper canopy of edges had significant PAI losses of 6.8% (-0.25 m^2 m^{-2}) in July (t = 2.2; P value < 0.05), nearly 3 months before the upper canopy of interior forests were significantly affected (Figure 3a).

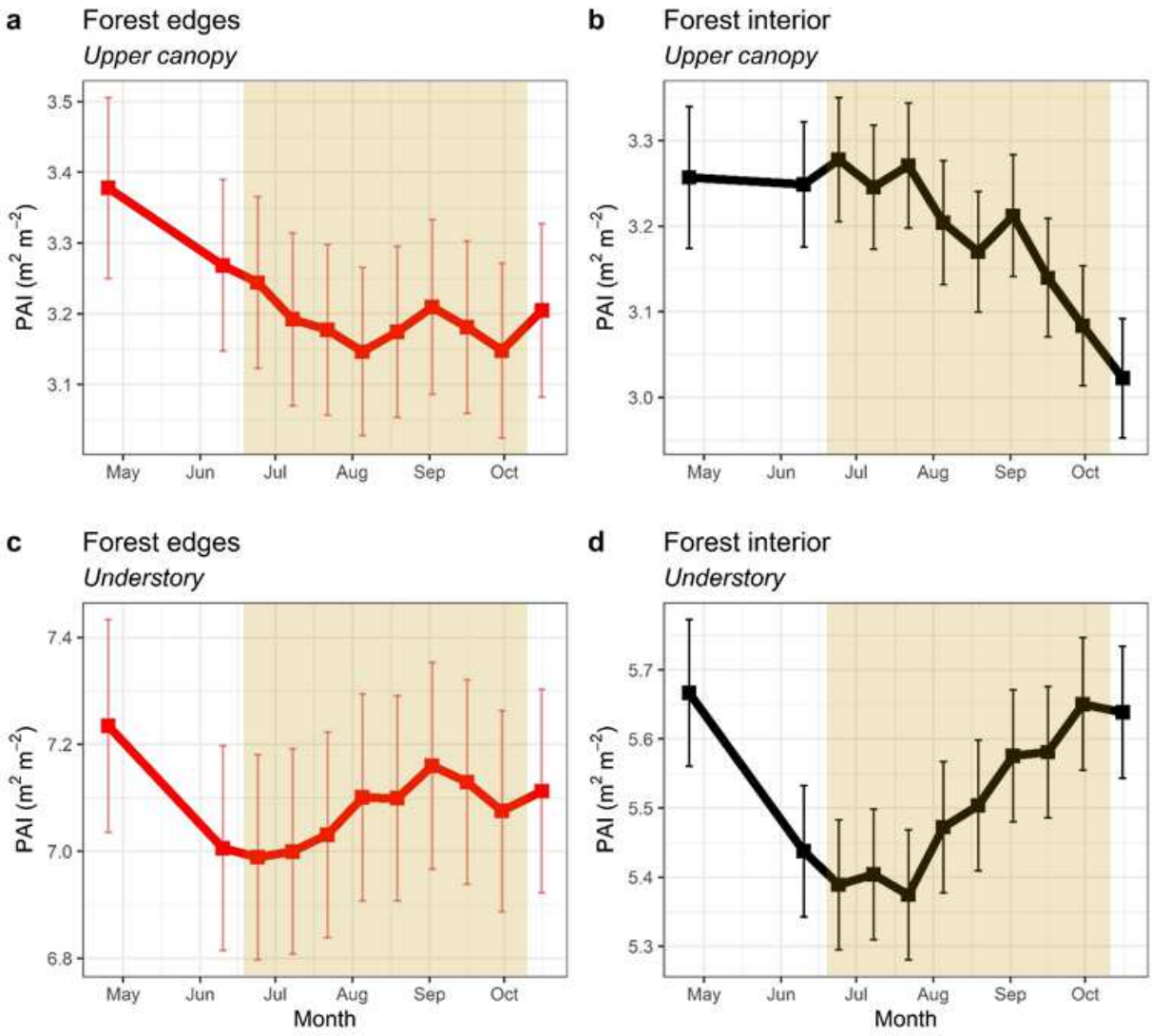

153

154 Figure 3. **Plant Area Index time-series.** Plant Area Index (PAI) predictions from linear mixed
155 modelling used date of LiDAR measurements and the interaction with a categorical variable
156 indicating whether plots were near an edge as fixed variables and transect as a random variable to
157 account for variation between transects (i.e. $PAI_{ij} = \beta_0 + \beta_1\ time_{ij} \times edge\ effects_{ij} + u_i + e_{ij}$).
158 Predicted PAI of the upper canopy ($\geq$ 15 m canopy height) in a) forest edges and b) undisturbed forest
159 interior, and predicted PAI of the understory (< 15 m canopy height) in c) forest edges and d)
160 undisturbed forest interior. Forest edges (in red) are defined as canopies within 40 m from forest
161 margins. Forest interior (in black) are canopies at least 40 m away from the forest fragment margins.
162 Each point represents the mean value predicted by mixed modelling, with the error bars depicting the
163 bootstrapped 95% confidence intervals. Dry season is defined when the accumulated monthly rainfall
164 is below 200 mm $month^{-1}$ with significant reductions in soil moisture.

165

We also illustrate the significant seasonal variations in PAI against the microclimatic conditions measured in the edges of the fragment and in the forest interior (Supplementary Figure 5, 6). The understory of interior forests had sharp decreases in PAI between April and June (Supplementary Figure 5b), a period when soil moisture was still high, and maximum temperatures were relatively low (27.8 $\pm$ 0.64 °C, Supplementary Figure 5d). The understory PAI of these forests increased alongside the increases in temperature during periods of high solar radiation, with a full recovery in plant area occurring when the temperatures peaked in September. On the other hand, losses in PAI of canopies on both edges and the forest interior occurred when temperatures were elevated (above 35 °C; Supplementary Figure 6d). Losses in PAI of upper canopies on the forest edges preceded canopy losses in the interior, which coincided with temperatures 3 - 5 °C hotter on edges throughout the dry season than interior environments (Supplementary Figure 6c); this strongly supports the idea that the seasonal dynamics of Amazonian forests at the upper canopy level is dependent on temperature, and that fragmentation exacerbates these effects.

We also investigate whether decreasing leaf area in the understory of forests on edges and in the forest interior was synchronised with variation in upper canopy plant area. We found a strongly negative linear correlation between variations in PAI of the upper canopy and understory in the forest interior (F-value = 54.4; P value < 0.001; R^2 = 0.84; Figure 4). There was not a relationship in edges (F-value = 1.2; P value = 0.29; R^2 = 0.02), which aligns with our hypothesis that fragmentation disrupts the seasonal patterns of understory dependency on upper canopy phenology.

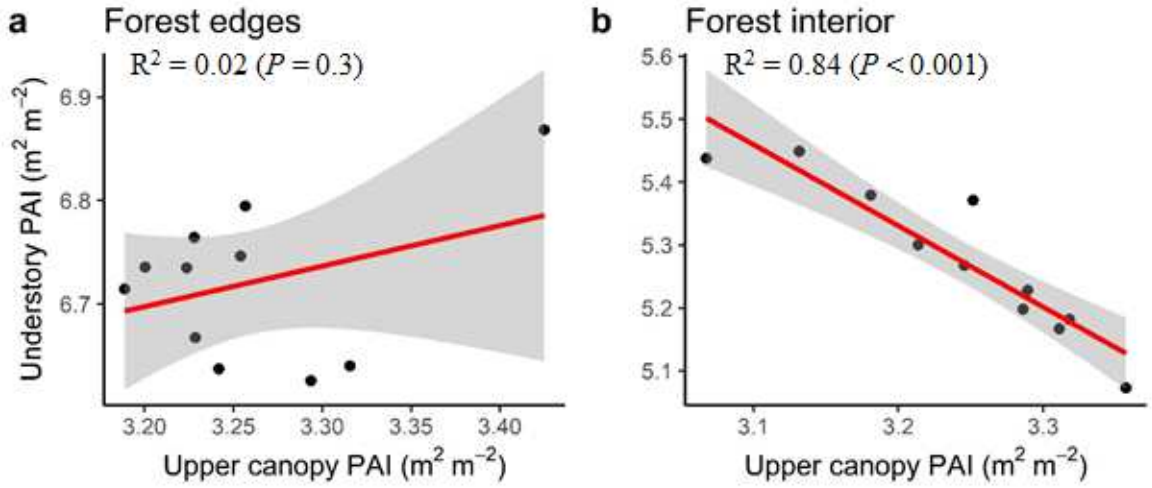

Figure 4. Correlation between seasonal changes in upper canopy PAI and understory PAI. LiDAR-based Plant Area Index (PAI, m^2 m^{-2}) between April and October 2019 from Central Amazonian

forests. Black dots represent the mean of all understory and upper canopy PAI values for each survey. The red lines represent values predicted by simple linear regression (i.e. Understory PAI = $\beta_0 + \beta_1$ Upper canopy PAI), with the shaded grey area depicting the 95% confidence intervals.

DISCUSSION

Repeat high-density terrestrial LiDAR combined with microclimate measurements in Amazonian forests provided a unique perspective on the seasonal dynamics of vegetation and the interaction with fragmentation. Plant area index, as a combination of leaf area index (LAI) and the area of woody components including trunks and branches, showed inverse patterns in the understory versus upper canopy. In the structurally undisturbed interior of a large forest fragment, plant area in the understory decreased by 5% before the start of the dry season and fully recovered by mid dry season in September. Conversely, the upper canopy (> 15 m aboveground) of these forests maintain their canopy structure throughout most of the dry season, with the greatest losses (8%) in upper canopy PAI occurring from September to mid-October when the microclimate of these forests reaches the lowest soil moisture and the maximum temperatures above 35 °C. Variations in plant area in the understory were strongly coordinated with upper canopy changes in PAI (R^2 = 85%, figure 4), which suggests that leaf flush in the understory follows increasing light availability as plant area is lost in the upper canopy. Edge effects, however, disrupted the seasonal trends in understory plant area and exacerbated upper canopy loss throughout the dry season. This pattern of higher leaf loss is consistent with edge effects enhancing leaf stress and creating periods of high evaporative demand - indeed, temperatures were mostly 3 - 5 °C higher and soil moisture levels lower in the dry season at the forest edge. The study demonstrates the value of repeated terrestrial LiDAR surveys, which allow the detection of fine-scale changes in forests without potential artefacts of passive remote sensing studies [42] and provide a perspective on forest dynamics and its spatial variability that is difficult to achieve with lower resolution remote sensing approaches.

Seasonal variation in plant area of intact Amazonian forests

Repeat terrestrial LiDAR measurements of PAI made every 15 days in Central Amazonian forests provide observations of the balance between new leaf development (flush of new leaves, plant growth) and loss to abscission (leaf and branch fall) that could be separated across forest strata. Our PAI time-series indicated that in old-growth forests distant from edges, higher loss in the upper

canopy occurs with elevated temperatures, whereas the understory maintains high leaf production under high light availability mediated by the upper canopy dynamics, even during periods of drier soil and atmospheric conditions. Passive remote sensing observations have demonstrated that Central Amazonian forests "green-up" during the dry season [9,11], but field measurements show negligible increases in PAI [4,12]. While our results agree that the total canopy PAI (the combined understory and upper canopy PAI) was not sensitive to climatic seasonality, our findings demonstrate stratified canopy responses to seasonally-mediated environmental conditions. These findings suggest that if differences between strata are not considered alongside changes in LAI, litterfall production and leaf demography, predictions of the climatic influences on vegetation may be undermined or misleading.

Vertical differences in phenology may arise from a direct response to higher light availability in the understory and from contrasting functional and hydraulic properties between canopy and understory trees. Recent studies in Amazonian forests have shown that leaf area increases in the understory occur under maximal irradiance conditions when the upper canopy layer is partially deciduous during the dry season [38,39], as diffuse and direct solar radiation in the understory can increase linearly with decreasing upper canopy plant area [56]. The dominant species in the understory of Amazonian forests are distinct from upper canopy dominants, and are differentiated and more complex in functional strategies [37,68]. Understory trees have xylem that is more embolism resistant and can tolerate more negative water potentials in the dry season without risking hydraulic failure compared to upper canopy trees, which tend to be more vulnerable to drought-induced embolism [32]. High embolism resistance of understory trees allows an anisohydric stomatal behaviour (low degree of regulation) and the maintenance of high stomatal conductance at the peak of the dry season [32]. The high drought tolerance of understory trees is also likely to be a key trait allowing them to flush new leaves during periods of water stress. In contrast, canopy trees exhibit lower embolism resistance, high stomatal sensitivity and significant declines in photosynthesis during periods of high atmospheric demand and low soil water availability [69]. The loss of upper canopy leaves in Amazonian forests at the end of the dry season is consistent with the importance of water availability for leaf development [38], and suggests that canopy trees in these forests may be vulnerable to periods of high evaporative demand [2,22].

Forest fragmentation disrupts seasonal patterns of plant area

We observed strong edge effects on phenology. Upper canopy PAI losses in forest edges occurred nearly three months before upper canopy losses in the forest interior and were significantly affected

by the dry season. Dry season temperatures in forest edges were 3 – 5 °C higher than in the interior of the fragment, but changes in soil moisture were small. These higher temperatures may lead to an increase in vapour pressure deficit (VPD), inducing stomatal closure and leaf loss [23,69,78,79], as shedding leaves may help to avoid the desiccating effects of water and heat stress [80]. On the other hand, plant area in the understory of forest edges was unaffected by higher temperatures or changes in upper canopy leaf area. The aseasonality of plant area in the understory of edges indicates that leaf production rates were similar to leaf loss rates during wet and dry seasons. These edges are dominated by pioneer species [25] that thrive under the light-rich environment caused by lateral light penetration and by the formation of gaps associated with the mortality of large trees [81]; these conditions may disrupt the between-strata light-mediated anticorrelation of leaf area dynamics since edge understories are less affected by the light intercepted by the upper canopy.

This study sheds light on the seasonal trends in plant area of Amazonian forests and highlights complex interacting effects of climate and human disturbance on forest phenology. The dry season losses in upper canopy leaf area—where large trees dominate—that we observed in fragment edges may supress total CO_2 uptake, with possible negative consequences for tree growth, and lower investment in tissue maintenance and defence [82]. Carbon losses from forest degradation already exceed those from deforestation in the Amazon [83], and fragmentation is a large contributor to degradation-associated carbon emissions [84]. Given the drier and warmer future projected for the Central and Eastern regions of the Amazon, and extended dry-season length [85], our findings suggest that fragmentation will exacerbate the negative effects of high temperatures on the upper canopy of these forests. Considering that fragment edges cover a total area of 176,555 km^2 of Amazonian forests [45], the sensitivity of these canopies on the edges of fragmented forests to high temperatures could translate into a large component of edge-related carbon losses.

METHODS

The study was conducted in Central Amazonian forests (2°20 30 ′S, 60° 05 37 W) within the Biological Dynamics of Forest Fragments Project (BDFFP), the world's longest-running experimental study of habitat fragmentation [44]. The region has seen notable carbon and biodiversity losses due to forest fragmentation effects [25,45] and is predicted to be markedly impacted by climatic changes [46]. The pioneering BDFFP project sites are composed of forest fragments originally isolated in 1980 by converting mature forest into cattle pastures. Currently, the matrix is dominated by

secondary growth forests, but a 100 m strip surrounding the forest fragments is regularly cleaned by cutting vegetation regrowth to keep the forest fragments isolated (Supplementary Figure 1a). As an experimental control that minimises anthropogenic influences as confounding factors, such as illegal logging, hunting, fire penetration and pollution, the project offers unique insights into ecological and environmental changes in fragmented forests. We selected a 100-ha forest fragment to investigate phenological responses with varying distances from the fragment edges (0 – 500 m). At the community level, the forest edges of our study are dominated by a high density of early-successional, fast-growth species, because of the elevated tree mortality near forest edges and seed dispersion from degraded neighbouring habitats, while the centre of the fragment comprises of undisturbed primary forests [25,44].

Terrestrial Laser Scanning: data acquisition, registration and Plant Area Index estimation

The TLS data were acquired using a RIEGL VZ-400i system between April and October 2019 every 15 days, except between the end of April and early June when the time difference between measurements was 40 days (we clarify in the analysis section how we addressed artefacts attributed to sampling effort). We used a scan resolution of 40 mDeg in both azimuth and zenith directions, which results in a point spacing of 34 mm at 50 m distance from the scanner. The laser pulse repetition rate used was 600 kHz, allowing a measurement range of up to 350 m and up to eight returns per pulse. The scans covered two transects of 100 x 10 m perpendicular to the forest fragment margins measured 11 times and 1 transect of 30 x 10 m length in the centre of the forest fragment measured 10 times. The transect in the centre lies 500 m from any fragment margin to ensure sampling of forest interior and that effectively there were no edge effects (this distance is much greater than detected edge effects in canopy structure of these fragments; Almeida *et al.* 2019c).

To ensure a full 3D representation of the upper canopy, each transect consisted of three scan lines parallel to each other with scans spaced at 5 m intervals within and between lines (Supplementary Figure 1b). The distance between scanning positions was smaller than the 10-40 m usually applied in previous studies to minimize data uncertainties due to occlusion in dense tropical forests and maximize data acquisition in the upper canopy [47]. Given that the RIEGL VZ-400i has a zenith angle range of 30–130°, an additional scan was acquired at each sampling location with the scanner tilted at 90° from the vertical position. A total of 276 scans across all transects each time resulted in a complete sampling of the full hemisphere in each scan location (Supplementary Figure 1c). All scans

were later co-registered into a single point cloud per transect using the RiSCAN PRO software, provided by RIEGL. Given that the RIEGL VZ-400i uses onboard sensor data with an algorithm to align scans without the use of reflectors, automatic registration was done before a final adjustment of scans.

To minimise errors in the fusion of the repeated scans, we first created a common digital terrain model (DTM) at 0.5 m resolution using a combination of ground returns from the first survey. Using an inverse distance weighting algorithm in the function *grid_terrain* in *lidR* in the software R, a common DTM was constructed from LiDAR ground returns. Plant area density (PAD) for all transects was then calculated using a voxel-based approach (with a 5 m buffer around each transect to maximise the PAD data). The volume occupied by vegetation within each transect was divided into 1 m^3 voxels, and the PAD calculated for each of these voxels (Supplementary Figure 1d). This procedure was done in the LiDAR data voxelization software AMAPVox [48,49]. AMAPvox tracks every laser pulse through a 3D grid (voxelized space) to the last recorded hit. The effective sampling area of each laser pulse (or fraction of pulse in case of multiple hits) is computed from the theoretical beam section (a function of distance to laser and divergence of laser beam) and the remaining beam fraction entering a voxel. In case more than one hit is recorded for a given pulse, the beam section is equally distributed between the different hits of the pulse. This information is combined with the optical path length of each pulse entering a voxel to compute the local transmittance or equivalently the local attenuation per voxel. Different estimation procedures are provided in the AMAPVox software. We used the Free Path Length estimator first developed for single return TLS in Pimont and colleagues [49] and later extended to the multiple return case [50]. The common assumption made for all estimation procedures in AMAPvox is to consider vegetation elements as randomly distributed within a voxel (thereby neglecting within voxel clumping) and to express the directional gap probability (or directional transmittance) as a function of the optical path length of laser pulse through a voxel and the local extinction coefficient [51]. The extinction coefficient is the product of the Plant Area Density and the projection function $G(\theta)$, which is the ratio of plant area projected in direction θ to actual area:

$$P(\theta , l) = \exp(- \lambda_\theta \times l), \qquad \text{(Eq. 1)}$$

where $P(\theta,l)$ is the probability of non-interception of a light beam of zenith angle θ (i.e. directional gap probability) along a path of length l, λ_θ (m^{-1}) is the directional attenuation coefficient, and l is the optical path length (m).

The *PAD* (m^2 m^{-3}) is related to λ as follow:

$PAD = \lambda_\theta / G(\theta)$ (Eq. 2)

G(θ), the plant projection function, is taken equal to 0.5, assuming a spherical distribution of leaf inclination angles [52]. This function is likely to be spatially variable in complex forest canopies.

We used a one cubic meter resolution to voxelise the canopy transects. In total, the number of voxels was 230,609, which were monitored 11 times during seasonal changes. We then calculated the sum of PADs for each 1 m^2 vertical column (X, Y coordinate) to obtain the Plant Area Index (PAI), which is a combination of the leaf area index and the area of wood components, including branches and trunks.

Determining edge effects and number of forest strata

To test the hypotheses that first fragmentation has significant effects on the structure of the vegetation in the BDFFP experiment — following Almeida and colleagues [53] — and second that edge effects also impact phenology, we related Plant Area Index (PAI) with edge distance in a nonlinear mixed model. We included $exp^{(-x)}$ as an asymptotic component that represents the saturation of PAI with distance from edge, denoted by x in the model, and transect as a random variable, allowing us to include any idiosyncratic differences between transects. This approach has been used to investigate edge effects on forest structure and dynamics [23,54]. A hockey-stick model consisting of two linear segments was also implemented with the R package hockeystick. This model identified a "distance from edge" threshold, dividing voxels into edge and interior groups (Supplementary Methods 2). We demonstrate that PAI varies within ~ 35 m of forest margins (Supplementary Fig. 2). These results corroborate a previous study in the same forest fragments showing edge effects of up to 40 m on canopy height [55]. Therefore, we considered edge in this study as the forests within 40 m of the forest fragment margins, which resulted in two edge transects (2 x 40 m) and three interior transects (2 x 60 m + 1 x 30 m).

We also tested the hypothesis suggested by Smith and colleagues [19] that the lower and upper strata of the vegetation have asynchronous changes in plant area during the dry season by comparing PAD on October 16th with PAD on June 24th in these strata. Species, functional and phylogenetic composition of the understory are distinct from the upper canopy in Central Amazonian forests [32,37]. While the understory is comprised of lower branches, seedlings, shade-tolerant and embolism resistant trees and

shrubs, lianas, acaulescent palms and saplings of young adult trees, the upper canopy is made up of adult predominantly shade-tolerant species, including tall and emergent trees and lianas. We then calculated the changes in PAD during the dry season to investigate shifts in the vertical profile of vegetation to elucidate the seasonal responses of specific strata (Supplementary Fig. 3a, 3b).

We observed consistent positive PAD changes below the height of 15 m above the ground and negative PAD changes above 15 m height (Supplementary Fig. 3b). Thus, given the existence of only two axes of variation along the vertical profile of the vegetation, we utilized this height to define understory (< 15 m aboveground) and upper canopy (≥ 15 m aboveground) in this study. This is consistent with a prior study in Amazonian forest, which also demonstrated distinct seasonal responses in leaf area above and below a height of 15 m [19]. The sum of all the understory PADs and the upper canopy PADs are referred to as understory PAI and upper canopy PAI, respectively. Our analysis comprises of 5,133 PAI values for the understory and 5,133 PAI values for the upper canopy, each monitored 11 times during the seasonal climatic variations. The understory accounts for 62 + 1.1 % of the total PAI in the forest interior, and 68 + 0.4 % of the total PAI of forest edges throughout the period of measurement (Supplementary Fig. 3a).

Climatic variables to elucidate the timing in PAI seasonal changes

PAI changes may be controlled by micro and macroclimatic conditions and changes [19,38,39]. We demonstrate below how we estimated solar radiation and accumulated rainfall at the landscape level, and continuously measured air temperature and soil moisture in the understory of forest edges and interior of forest fragments to examine the synchrony between these factors and the PAI time-series in the understory and canopy.

Solar radiation and accumulated rainfall

Leaf flushing in Central Amazonian forests coincides with peaks in Photosynthetic Active Radiation (PAR, W/m^2) during periods of low rainfall [4,14,38]. PAR varies significantly within forest canopies and changes over time due to variations in the incident solar flux density and solar direction [56]. Incident solar PAR contains two components: direct PAR and diffuse PAR – and the latter is mostly controlled by scattering of particles and cloud cover in the atmosphere [57]. The photosynthetic efficiencies of direct and diffuse PAR are different in forests, with positive effects of diffuse light on

photosynthetic rates [58] and atmospheric CO_2 assimilation [59] in comparison to plants under direct light conditions. To examine the synchrony between PAR and seasonal PAI changes, we derived solar radiation from the product MCD18A2 V6 (https://lpdaac.usgs.gov/products/mcd18a2v006/). This product uses the bands of the visible spectrum (400 – 700 nm) of both sensors (Terra and Aqua) from the Moderate Resolution Imaging Spectroradiometer (MODIS) to estimate daily PAR at a 5-kilometer pixel resolution [60]. Daily mean rainfall estimates were also derived from the NASA's POWER (Prediction of Worldwide Energy Resources) data with a spatial resolution of 0.5° latitude by 0.5° longitude (55 x 55 km). Meteorological parameters are derived from the NASA's GMAO MERRA-2 assimilation model (https://gmao.gsfc.nasa.gov/reanalysis/MERRA/) and GEOS FP-IT (https://gmao.gsfc.nasa.gov/news/geos_system_news/2016/FP-IT_NRT_G5.12.4.php). We then integrated the daily rainfall estimates to accumulated monthly (30-day period) rainfall and classified dry season as the period with running 30-day rainfall below 200 mm as in Maeda and colleagues [61].

Microclimate variables

Soil moisture and maximum temperatures are key drivers of species' distributions and affect how species respond to climatic variations [62,63]. We measured air temperature (°C) and electrical conductivity of soil moisture (time-domain transmission; TDT) across a network of 22 data loggers varying in distance from the forest fragment margins (0 and 520 m). Temperature-Moisture-Sensor (TMS) data loggers measured air temperature at 15 cm above the ground and TDT at 8 cm below ground [64]. TDT values were transformed into volumetric soil moisture following calibration curves in Wild and colleagues [64] using as input data soil texture (50 % clay, 25% sand and 25% silt contents) and mean soil density of 1100 kg/m^3 measured by Camargo and Kapos [65] in the same forest fragments of our study. Data loggers were shielded from direct solar radiation and recorded data every 15 minutes. Microclimate data were recorded between 27th April 2019 and 16th October 2019, resulting in a total of 435798 coupled temperature and volumetric soil moisture readings. TMS device measures microclimate variables affecting many ecological processes, including those related to water and energy balance. We calculated mean daily soil moisture and maximum daily soil moisture to investigate their synchrony with the PAI time-series.

Phenology modelling for interior and edge forests We used a linear mixed-effects (LME) model of understory PAI, upper canopy PAI and a combination of both strata (total PAI) measured from

435 TLS in each transect as a function of time of measurement (*time*). We included an interaction term
436 with the plot category of location near an edge or in the forest fragment interior (*edge effects*)
437 following Qie and colleagues [54]. The *time* × *edge effects* interaction represents how edge effects
438 caused by forest fragmentation influence the seasonal variation in PAI. We performed χ^2 tests to
439 compare this LME model with other LME models that contained the variables *time*, *edge effects* and
440 an interaction term *time* x *edge effects* to examine the significance of seasonality and fragmentation
441 on PAI variation (Supplementary Table 1). χ^2-tests and *P* values were performed by comparing to
442 random-intercept models of the form PAI~ 1 + (1| Transect) and model explanatory power was
443 assessed in terms of AIC. Transect identity was included as a random effect, allowing us to include
444 any idiosyncratic differences between transects, with a random intercept term capturing variation in
445 PAI between transects. The LME model was fitted using the *lme* function in the *nlme* R package.
446 Variations in transect area and monitoring period can influence PAI trends, and we used
447 *varIdent* weights function to account for the noise attributed to sampling effort [66]. We then used the
448 function *bootstrap* to perform model-based semi-parametric bootstrap to estimate the LME
449 parameters and 95% confidence intervals.

450 If increasing upper canopy PAI contributes to lower light interception in the lower stratum of the
451 vegetation, we may expect a decreasing leaf development in the understory of forests in the interior
452 of fragments [38,56]. However, we may also expect that such an effect on understory PAI by increasing
453 upper canopy PAI is reduced or absent near fragment edges, with the loss of tall trees and lateral light
454 from forest edges exposing the understory to more direct sunlight [67]. We tested this by averaging the
455 community-level PAI in understory and upper canopy strata for each census, and then using linear
456 models (*lm* function in R) to examine the relationships of PAI between the understory and upper
457 canopy.

458

459 **ACKNOWLEDGEMENTS**

460 This study was funded by the Academy of Finland (decision numbers 318252, 319905 and 345472).
461 This publication is number XXX of the Technical Series of the Biological Dynamics of Forest
462 Fragment Forest (BDFFP – INPA / STRI). We thank the Biological Dynamics of Forest Fragment
463 Project for logistical support in the field. We are grateful to Renann Dias Silva, Juliane Menezes and
464 Vinicius Bertin for the great assistance in the field. S.C.S. received support from the US NSF (DEB-
465 1950080 and 1754357) and USDA NIFA. G.V. received support from Laboratoire d'Excellence
466 CEBA (ANR-10-LABX-25). Y.M.M. was supported by the Royal Society under the Newton

International Fellowship funding (NF170036) and HPC-Europa-3 (HPC17TA3RL), supported by H2020-European Commission.

AUTHOR CONTRIBUTIONS

E.E.M, J.L.C.C and M.H.N conceived of the project. E.E.M and M.H.N led data collection. E.E.M and G.V processed the LiDAR data. M.H.N performed data analyses and wrote the manuscript. All authors contributed to the revision of the paper.

COMPETING INTERESTS

The authors declare no competing interests.

REFERENCES

1. Peñuelas, J., Rutishauser, T. & Filella, I. Ecology. Phenology feedbacks on climate change. *Science* **324**, 887–888 (2009).

2. Phillips, O. L. *et al.* Drought sensitivity of the Amazon rainforest. *Science* **323**, 1344–1347 (2009).

3. Richardson, A. D. *et al.* Climate change, phenology, and phenological control of vegetation feedbacks to the climate system. *Agric. For. Meteorol.* **169**, 156–173 (2013).

4. Wu, J. *et al.* Leaf development and demography explain photosynthetic seasonality in Amazon evergreen forests. *Science* **351**, 972–976 (2016).

5. Wright, J. S. *et al.* Rainforest-initiated wet season onset over the southern Amazon. *Proc. Natl. Acad. Sci. U. S. A.* **114**, 8481–8486 (2017).

6. Hilker, T. *et al.* Vegetation dynamics and rainfall sensitivity of the Amazon. *Proc. Natl. Acad. Sci. U. S. A.* **111**, 16041–16046 (2014).

7. Girardin, C. A. J. *et al.* Seasonal trends of Amazonian rainforest phenology, net primary productivity, and carbon allocation. *Global Biogeochem. Cycles* **30**, 700–715 (2016).

8. Maeda, E. E. *et al.* Consistency of vegetation index seasonality across the Amazon rainforest. *Int. J. Appl. Earth Obs. Geoinf.* **52**, 42–53 (2016).

9. Saleska, S. R. *et al.* Dry-season greening of Amazon forests. *Nature* vol. 531 E4–5 (2016).

10. Chen, X. *et al.* Vapor pressure deficit and sunlight explain seasonality of leaf phenology and photosynthesis across amazonian evergreen broadleaved forest. *Global Biogeochem. Cycles* **35**, (2021).

11. Hashimoto, H. *et al.* New generation geostationary satellite observations support seasonality in greenness of the Amazon evergreen forests. *Nat. Commun.* **12**, 684 (2021).

12. Brando, P. M. *et al.* Seasonal and interannual variability of climate and vegetation indices across the Amazon. *Proc. Natl. Acad. Sci. U. S. A.* **107**, 14685–14690 (2010).

13. Wu, J. *et al.* Seasonality of Central Amazon Forest Leaf Flush Using Tower-Mounted RGB Camera. in vol. 2014 B11G–0107 (2014).

14. Huete, A. R. *et al.* Amazon rainforests green-up with sunlight in dry season. *Geophys. Res. Lett.* **33**, (2006).

15. Restrepo-Coupe, N. *et al.* What drives the seasonality of photosynthesis across the Amazon basin? A cross-site analysis of eddy flux tower measurements from the Brasil flux network. *Agric. For. Meteorol.* **182-183**, 128–144 (2013).

16. Manoli, G., Ivanov, V. Y. & Fatichi, S. Dry-season greening and water stress in Amazonia: The role of modeling leaf phenology. *J. Geophys. Res. Biogeosci.* **123**, 1909–1926 (2018).

17. Guan, K. *et al.* Photosynthetic seasonality of global tropical forests constrained by hydroclimate. *Nat. Geosci.* **8**, 284–289 (2015).

18. Lopes, A. P. *et al.* Leaf flush drives dry season green-up of the Central Amazon. *Remote Sens. Environ.* **182**, 90–98 (2016).

19. Smith, M. N. *et al.* Seasonal and drought-related changes in leaf area profiles depend on height and light environment in an Amazon forest. *New Phytol.* **222**, 1284–1297 (2019).

518 20. Mitchell Aide, T. Herbivory as a selective agent on the timing of leaf production in a tropical
519 understory community. *Nature* **336**, 574–575 (1988).

520 21. Myneni, R. B. *et al.* Large seasonal swings in leaf area of Amazon rainforests. *Proc. Natl.*
521 *Acad. Sci. U. S. A.* **104**, 4820–4823 (2007).

522 22. Wu, J. *et al.* Partitioning controls on Amazon forest photosynthesis between environmental and
523 biotic factors at hourly to interannual timescales. *Glob. Chang. Biol.* **23**, 1240–1257 (2017).

524 23. Nunes, M. H. *et al.* Recovery of logged forest fragments in a human-modified tropical
525 landscape during the 2015-16 El Niño. *Nat. Commun.* **12**, 1526 (2021).

526 24. Vasconcelos, H. L. & Luizão, F. J. Litter production and litter nutrient concentrations in a
527 fragmented amazonian landscape. *Ecol. Appl.* **14**, 884–892 (2004).

528 25. Laurance, W. F. *et al.* Rain forest fragmentation and the proliferation of successional trees.
529 *Ecology* **87**, 469–482 (2006).

530 26. Uriarte, M. *et al.* Impacts of climate variability on tree demography in second growth tropical
531 forests: the importance of regional context for predicting successional trajectories. *Biotropica*
532 **48**, 780–797 (2016).

533 27. Ewers, R. M. & Banks-Leite, C. Fragmentation impairs the microclimate buffering effect of
534 tropical forests. *PLoS One* **8**, e58093 (2013).

535 28. Chave, J. *et al.* Regional and seasonal patterns of litterfall in tropical South America.
536 *Biogeosciences* **7**, 43–55 (2010).

537 29. de Moura, Y. M. *et al.* Spectral analysis of amazon canopy phenology during the dry season
538 using a tower hyperspectral camera and modis observations. *ISPRS J. Photogramm. Remote*
539 *Sens.* **131**, 52–64 (2017).

540 30. Nunes, M. H. *et al.* Changes in leaf functional traits of rainforest canopy trees associated with
541 an El Niño event in Borneo. *Environ. Res. Lett.* **14**, 085005 (2019).

542 31. Barros, F. de V. *et al.* Hydraulic traits explain differential responses of Amazonian forests to
543 the 2015 El Niño-induced drought. *New Phytol.* **223**, 1253–1266 (2019).

32. Brum, M. *et al.* Hydrological niche segregation defines forest structure and drought tolerance strategies in a seasonal Amazon forest. *J. Ecol.* **107**, 318–333 (2019).

33. Signori-Müller, C. *et al.* Non-structural carbohydrates mediate seasonal water stress across Amazon forests. *Nat. Commun.* **12**, 2310 (2021).

34. Coelho de Souza, F. *et al.* Evolutionary heritage influences Amazon tree ecology. *Proc. Biol. Sci.* **283**, (2016).

35. Hansen, M. C. *et al.* The fate of tropical forest fragments. *Sci Adv* **6**, eaax8574 (2020).

36. Morton, D. C. *et al.* Amazon forests maintain consistent canopy structure and greenness during the dry season. *Nature* **506**, 221–224 (2014).

37. Draper, F. C. *et al.* Amazon tree dominance across forest strata. *Nat Ecol Evol* (2021) doi:10.1038/s41559-021-01418-y.

38. Tang, H. & Dubayah, R. Light-driven growth in Amazon evergreen forests explained by seasonal variations of vertical canopy structure. *Proc. Natl. Acad. Sci. U. S. A.* **114**, 2640–2644 (2017).

39. Correction for Tang and Dubayah, Light-driven growth in Amazon evergreen forests explained by seasonal variations of vertical canopy structure. *Proc. Natl. Acad. Sci. U. S. A.* **116**, 9137 (2019).

40. Tang, H., Dubayah, R., Brolly, M., Ganguly, S. & Zhang, G. Large-scale retrieval of leaf area index and vertical foliage profile from the spaceborne waveform lidar (GLAS/ICESat). *Remote Sens. Environ.* **154**, 8–18 (2014).

41. Almeida, D. R. A. de *et al.* Optimizing the Remote Detection of Tropical Rainforest Structure with Airborne Lidar: Leaf Area Profile Sensitivity to Pulse Density and Spatial Sampling. *Remote Sensing* **11**, 92 (2019).

42. Calders, K. *et al.* Monitoring spring phenology with high temporal resolution terrestrial LiDAR measurements. *Agric. For. Meteorol.* **203**, 158–168 (2015).

43. Disney, M. Terrestrial LiDAR: a three-dimensional revolution in how we look at trees. *New Phytol.* **222**, 1736–1741 (2019).

571 44. Laurance, W. F. *et al.* An Amazonian rainforest and its fragments as a laboratory of global
572 change. *Biol. Rev. Camb. Philos. Soc.* **93**, 223–247 (2018).

573 45. Silva Junior, C. H. L. *et al.* Persistent collapse of biomass in Amazonian forest edges following
574 deforestation leads to unaccounted carbon losses. *Sci Adv* **6**, (2020).

575 46. Nobre, C. A. *et al.* Land-use and climate change risks in the Amazon and the need of a novel
576 sustainable development paradigm. *Proc. Natl. Acad. Sci. U. S. A.* **113**, 10759–10768 (2016).

577 47. Wilkes, P. *et al.* Data acquisition considerations for Terrestrial Laser Scanning of forest plots.
578 *Remote Sens. Environ.* **196**, 140–153 (2017).

579 48. Vincent, G. *et al.* Mapping plant area index of tropical evergreen forest by airborne laser
580 scanning. A cross-validation study using LAI2200 optical sensor. *Remote Sens. Environ.* **198**,
581 254–266 (2017).

582 49. Pimont, F., Allard, D., Soma, M. & Dupuy, J.-L. Estimators and confidence intervals for plant
583 area density at voxel scale with T-LiDAR. *Remote Sens. Environ.* **215**, 343–370 (2018).

584 50. Vincent, G., Pimont, F. & Verley, P. A note on PAD/LAD estimators implemented in
585 AMAPVox 1.7. (2021) doi:10.23708/1AJNMP.

586 51. Ross, J. *The radiation regime and architecture of plant stands*. (Springer, Dordrecht, 1981).

587 52. Béland, M., Widlowski, J.-L., Fournier, R. A., Côté, J.-F. & Verstraete, M. M. Estimating leaf
588 area distribution in savanna trees from terrestrial LiDAR measurements. *Agric. For. Meteorol.*
589 **151**, 1252–1266 (2011).

590 53. Almeida, D. R. A. *et al.* Persistent effects of fragmentation on tropical rainforest canopy
591 structure after 20 yr of isolation. *Ecol. Appl.* **29**, e01952 (2019).

592 54. Qie, L. *et al.* Long-term carbon sink in Borneo's forests halted by drought and vulnerable to
593 edge effects. *Nat. Commun.* **8**, 1966 (2017).

594 55. Almeida, D. R. A. *et al.* Persistent effects of fragmentation on tropical rainforest canopy
595 structure after 20 yr of isolation. *Ecol. Appl.* **29**, e01952 (2019).

596 56. Ma, L. *et al.* Characterizing the three-dimensional spatiotemporal variation of forest
597 photosynthetically active radiation using terrestrial laser scanning data. *Agric. For. Meteorol.*
598 **301-302**, 108346 (2021).

599 57. Росс, Ю. & Ross, J. *The radiation regime and architecture of plant stands*. (Springer Science
600 & Business Media, 1981).

601 58. Berry, Z. C. & Goldsmith, G. R. Diffuse light and wetting differentially affect tropical tree leaf
602 photosynthesis. *New Phytol.* **225**, 143–153 (2020).

603 59. Mercado, L. M. *et al.* Impact of changes in diffuse radiation on the global land carbon sink.
604 *Nature* **458**, 1014–1017 (2009).

605 60. LP DAAC - MCD18A1. https://lpdaac.usgs.gov/products/mcd18a1v006/.

606 61. Maeda, E. E. *et al.* Large-scale commodity agriculture exacerbates the climatic impacts of
607 Amazonian deforestation. *Proc. Natl. Acad. Sci. U. S. A.* **118**, (2021).

608 62. Engelbrecht, B. M. J. *et al.* Drought sensitivity shapes species distribution patterns in tropical
609 forests. *Nature* **447**, 80–82 (2007).

610 63. Zellweger, F. *et al.* Forest microclimate dynamics drive plant responses to warming. *Science*
611 **368**, 772–775 (2020).

612 64. Wild, J. *et al.* Climate at ecologically relevant scales: A new temperature and soil moisture
613 logger for long-term microclimate measurement. *Agric. For. Meteorol.* **268**, 40–47 (2019).

614 65. Camargo, J. L. C. & Kapos, V. Complex Edge Effects on Soil Moisture and Microclimate in
615 Central Amazonian Forest. *J. Trop. Ecol.* **11**, 205–221 (1995).

616 66. Zuur, A., Ieno, E. N., Walker, N., Saveliev, A. A. & Smith, G. M. *Mixed Effects Models and*
617 *Extensions in Ecology with R*. (Springer Science & Business Media, 2009).

618 67. Malhi, Y., Phillips, O. L. & Laurance, W. F. Forest-climate interactions in fragmented tropical
619 landscapes. *Philos. Trans. R. Soc. Lond. B Biol. Sci.* **359**, 345–352 (2004).

620 68. Laurans, M., Hérault, B., Vieilledent, G. & Vincent, G. Vertical stratification reduces
621 competition for light in dense tropical forests. *For. Ecol. Manage.* **329**, 79–88 (2014).

622 69. Garcia, M. N. *et al.* Importance of hydraulic strategy trade-offs in structuring response of
623 canopy trees to extreme drought in central Amazon. *Oecologia* (2021) doi:10.1007/s00442-
624 021-04924-9.

625 70. Stark, S. C. *et al.* Amazon forest carbon dynamics predicted by profiles of canopy leaf area and
626 light environment. *Ecol. Lett.* **15**, 1406–1414 (2012).

627 71. Pyle, E. H. *et al.* Dynamics of carbon, biomass, and structure in two Amazonian forests. *J.*
628 *Geophys. Res.* **113**, (2008).

629 72. Gorgens, E. B. *et al.* Resource availability and disturbance shape maximum tree height across
630 the Amazon. *Glob. Chang. Biol.* **27**, 177–189 (2021).

631 73. Oliveira, R. S. *et al.* Embolism resistance drives the distribution of Amazonian rainforest tree
632 species along hydro-topographic gradients. *New Phytol.* **221**, 1457–1465 (2019).

633 74. Falster, D. S. & Westoby, M. Leaf size and angle vary widely across species: what
634 consequences for light interception? *New Phytol.* **158**, 509–525 (2003).

635 75. Chavana-Bryant, C. *et al.* Leaf aging of Amazonian canopy trees as revealed by spectral and
636 physiochemical measurements. *New Phytol.* **214**, 1049–1063 (2017).

637 76. Brando, P. M. *et al.* Drought effects on litterfall, wood production and belowground carbon
638 cycling in an Amazon forest: results of a throughfall reduction experiment. *Philos. Trans. R.*
639 *Soc. Lond. B Biol. Sci.* **363**, 1839–1848 (2008).

640 77. Wang, D., Momo Takoudjou, S. & Casella, E. LeWoS: A universal leaf-wood classification
641 method to facilitate the 3D modelling of large tropical trees using terrestrial LiDAR. *Methods*
642 *Ecol. Evol.* **11**, 376–389 (2020).

643 78. Grossiord, C. *et al.* Plant responses to rising vapor pressure deficit. *New Phytol.* **226**, 1550–
644 1566 (2020).

645 79. Smith, M. N. *et al.* Empirical evidence for resilience of tropical forest photosynthesis in a
646 warmer world. *Nat Plants* **6**, 1225–1230 (2020).

647 80. Aleixo, I. *et al.* Amazonian rainforest tree mortality driven by climate and functional traits.
648 *Nat. Clim. Chang.* **9**, 384–388 (2019).

81. Lohbeck, M. *et al.* Successional changes in functional composition contrast for dry and wet tropical forest. *Ecology* **94**, 1211–1216 (2013).

82. Doughty, C. E. *et al.* Drought impact on forest carbon dynamics and fluxes in Amazonia. *Nature* **519**, 78–82 (2015).

83. Qin, Y. *et al.* Carbon loss from forest degradation exceeds that from deforestation in the Brazilian Amazon. *Nat. Clim. Chang.* 1–7 (2021).

84. Brinck, K. *et al.* High resolution analysis of tropical forest fragmentation and its impact on the global carbon cycle. *Nat. Commun.* **8**, 14855 (2017).

85. Duffy, P. B., Brando, P., Asner, G. P. & Field, C. B. Projections of future meteorological drought and wet periods in the Amazon. *Proc. Natl. Acad. Sci. U. S. A.* **112**, 13172–13177 (2015).

86. Forrest, J. & Miller-Rushing, A. J. Toward a synthetic understanding of the role of phenology in ecology and evolution. *Philos. Trans. R. Soc. Lond. B Biol. Sci.* **365**, 3101–3112 (2010).

87. Park, J. Y. *et al.* Quantifying Leaf Phenology of Individual Trees and Species in a Tropical Forest Using Unmanned Aerial Vehicle (UAV) Images. *Remote Sensing* **11**, 1534 (2019).

88. Dubayah, R. *et al.* The Global Ecosystem Dynamics Investigation: High-resolution laser ranging of the Earth's forests and topography. *Egypt. J. Remote Sens. Space Sci.* **1**, 100002 (2020).

89. Calders, K. *et al.* Terrestrial laser scanning in forest ecology: Expanding the horizon. *Remote Sens. Environ.* **251**, 112102 (2020).

90. Malhi, Y. *et al.* New perspectives on the ecology of tree structure and tree communities through terrestrial laser scanning. *Interface Focus* **8**, 20170052 (2018).

Supplementary Files

This is a list of supplementary files associated with this preprint. Click to download.

- SupplementaryInformation.pdf